Supplementary Information

Great Oxidation and Lomagundi events linked by deep cycling and enhanced degassing of carbon

James Eguchi[1,2], Johnny Seales[1], Rajdeep Dasgupta[1]

[1]Department of Earth, Environmental and Planetary Sciences, Rice University, 6100 Main Street, MS-126, Houston, TX 77005

[2]Current Address: Department of Earth and Planetary Sciences, University of California, Riverside, 900 University Ave., Riverside, CA 92521

Quantifying organic carbon release in partial melts with different compositions

In Fig. 2c graphite solubility was calculated for a single, specific sediment partial melt composition using the model of Duncan and Dasgupta[27]. However, Duncan and Dasgupta[27] based their calculations on the assumption that a rhyolitic melt composition, identical to their experiments apply to all subduction zones – present and past – as the agent of CO_2 dissolution from graphite-saturated crustal lithologies. This assumption may not hold if TTG-type sediment compositions are more relevant for ancient subductions. To accommodate compositional diversity of downgoing sediments, and thus variation of hydrous melt compositions that dissolve CO_2 from graphite-saturated sediments, we use a recent model from Eguchi and Dasgupta[55], which can be used to calculate CO_2 solubility in graphite-saturated silicate melts for any given composition. In our calculations of graphite/diamond dissolution in silicate melts we use the same *P-T* paths and fO_2 used in Fig. 2. We performed our calculations for three different silicate melt compositions (Supplementary Table 4) that span the plausible compositions of hydrous

silicic melt generated from different crustal sediments. Organic C removal efficiency would be even lower if more reduced slab conditions are used, *i.e.,* the fO_2 conditions used give the highest CO_2 dissolution capacity and graphite/diamond saturation. Supplementary Fig. 1 demonstrates that even after considering a wide range of silicate melt compositions, our conclusion that graphitized organic C is likely to remain in the subducting slab remains unchanged.

Factors affecting shape and magnitude of oxygen increase and carbon isotope excursion

In supplementary Fig. 2a,b we explore the effects of variable release efficiency of carbonates and graphitized organic carbon at sub-arc depths. For carbonate release efficiency we vary α_{carb} from 1.0 to 0.6 (supplementary Fig. 2a), corresponding to 100% to 60% of subducted carbonates being released at arcs, with the remainder being released later at ocean islands. Decreasing α_{carb} (decreasing the fraction of carbonates released at arcs) decreases the magnitude of the C isotope excursion in carbonates. This covers the plausible range of values suggested by Fig. 2, save for the coldest subduction zones, in which there will be negligible carbonate as well as organic C release. We vary α_{org} from 0.0 to 0.4 (supplementary Fig. 2b), which corresponds to 0% to 40% of subducted organic C being released at arcs, with the remainder being released later at ocean islands. Increasing α_{org} from 0.0 to 0.4 (releasing more organic C at arcs) decreases the magnitude of the C isotope excursion in carbonates. This covers the plausible range of organic C release efficiency suggested by calculations shown in Fig. 2 and supplementary Fig. 1.

In supplementary Fig 2c we investigate how changing the fraction of C that remains in the crustal reservoir versus that being subducted affects the model output. In the model, the fraction of C that remains in the crustal reservoir is controlled by the parameter χ. In supplementary Fig. 1c we vary χ from 0.8 to 0.4, which represent 80% to 40% of carbonates and organic C produced being subducted into the mantle. Decreasing the amount of C that gets

subducted into the mantle decreases the magnitude of the C isotope excursion in carbonates. Supplementary Fig. 2c demonstrates that if 80% of carbonates are subducted the model closely reproduces the magnitude of the observed C isotope excursion.

In supplementary Fig. 2d we investigate the effect of varying the length of time required for organic C to be released at ocean islands. We investigate delay times of 200-500 Myr based upon the reasoning that subducted crust would travel ~10,000 km (down ~3000km, horizontally along core-mantle boundary ~3000 km, then up 3000 km) on its path from subduction to release at ocean islands at rates of ~2-10 cm/yr. This covers most of the range suggested for mantle convection velocities. These values assume that subducted crust does not accumulate at the core-mantle boundary for significant time periods, which has been shown by modeling studies of mantle convection[32]. Increasing the delay time of organic C release at ocean island volcanoes causes the C isotope excursion in carbonates to become more long-lived.

In supplementary Fig. 2e we show how varying the magnitude of increases in mid-ocean ridge CO_2 emissions affects the magnitude of the C isotope excursion. When the magnitudes of CO_2 emission increases are small, then larger magnitudes of CO_2 emission increases result in larger C isotope excursions. However, when the change to CO_2 emissions are greater than about 100-fold then any further increase in the magnitude of CO_2 increase does not result in a larger C isotope excursion (See Supp. Fig. 2e). This is most likely due to forcing model changes by changing CO_2 at mid-ocean ridges, which have $\delta^{13}C$ fixed at -5‰. When the increase of CO_2 emissions at mid-ocean ridges are large, they will play a more prominent role in controlling $\delta^{13}C_{carb}$ and will cap the magnitude of the C isotope excursion. In the current model design, the C isotope excursion does not reach the peak values observed in the geologic record, except when the amount of C subducted is high (Supp. Fig. 2c). This could be an artifact of forcing model

changes by only increasing CO_2 emissions at mid-ocean ridges. Additionally, we cannot rule out that small changes to f_{org} could have contributed the overall magnitude of the modeled C isotope excursion.

Adjusting CO_2 emissions to present-day estimates

We would like to emphasize that some of the ranges of values discussed above may be highly uncertain, and the equations used may be simplistic (Eq. 5). However, tighter constraints and added model complexity are unlikely to change the general behavior of the model. Rather, they would have small effects on the magnitudes of the behavior observed in the present model. To be clear, the goal of the present study is not to accurately reproduce the precisely recorded pCO_2 record for more recent time periods (*i.e.*, refs. [56, 57]). Many of the parameters for the time period we are investigating are poorly constrained so it may be unwarranted to attempt to more precisely reproduce the natural data with models of added complexity. Here, we seek only to demonstrate that with the new suggestions in this contribution that the present model can drive increased atmospheric oxygen and a positive carbon isotope excursion which are of the same orders of magnitude as the natural data. Future studies may investigate how adding more complexities to the surface carbon cycle affect model behavior, but that is beyond the scope of the present study.

However, as a test of the robustness of the present model, we increased the MORB emissions a second time to 10^{16} g C/Myr (3 order of magnitude increase), close to present-day estimates[41]. In Fig. 5 increased oxygen and the carbon isotope excursion are driven by increasing MOR CO_2 emissions by 3 orders of magnitude. Using geodynamic mantle convection models coupled with mantle melting, Fuentes et al.[14] demonstrate that an abrupt transition from sluggish

lid to plate tectonics could increase the flux of CO_2/m of mid-ocean ridges by a factor of ~10. If the transition is accompanied by an increase in ridge and arc length as is expected in a stagnant lid to mobile lid transition, the modeled factor of 10 can easily increase by orders of magnitude. Therefore, we argue that the 3 order of magnitude increases in MOR CO_2 emissions used to drive the changes in Fig. 5 and supplementary Fig. 3 are reasonable for major tectonic transitions such as sluggish/stagnant lid to plate tectonic transition. Similarly, the second major increase in MOR CO_2 emissions could have been driven by increased plate tectonic activity, which has been suggested at the end of the Proterozoic[17,24,45]. With present day C fluxes, the model predicts O_2 close to present-day levels. Additionally, the model predicts C reservoir sizes and fluxes, which are within 1-2 orders of magnitude of present-day estimates, *i.e.*, the model predicts an atmosphere-ocean C reservoir size on the order of 10^{19} g compared to actual estimates of ~4×10^{19} g (Ref.[58]), and the model predicts a weathering flux on the order of 10^{19} g C/Myr compared to actual estimates on the order of 10^{19} g C/Myr (Ref.[59]). Although, the model was not designed for this, the fact that using present-day MOR fluxes results in reasonable C reservoir gives us confidence that the model is an acceptable representation of the natural C cycle.

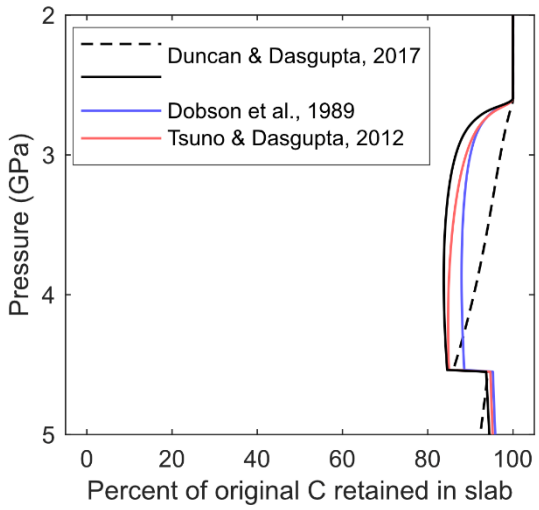

Supplementary Figure 1 Amount of subducted C retained in slab during the partial melting of graphite-saturated lithologies of different compositions. Dashed black curve shows how much C will be retained in the subducting slab when a sediment melt with intermediate SiO_2 and high alkali contents is produced (Calculated with model of Duncan and Dasgupta[27]) (Same as average curve in Fig. 2c). Solid black curve is calculated with the same composition, but using the solubility model of Eguchi and Dasgupta[55]. Blue and orange curves show much C will be retained in the subducting slab when sediment melts with high and low SiO_2 contents, respectively, are produced (Calculated with model of Eguchi and Dasgupta[55]). Melt compositions given in Supplementary Table 4.

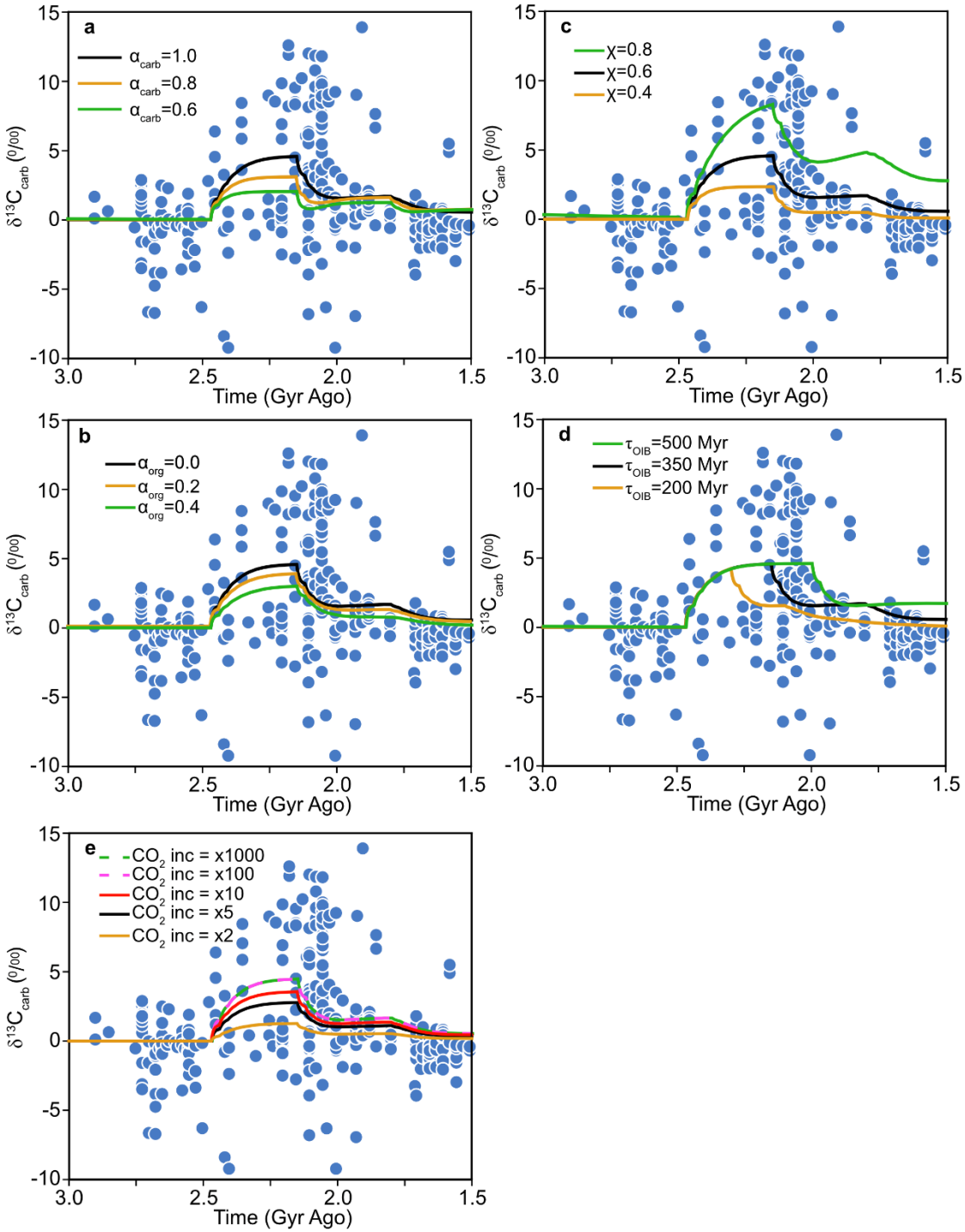

119

120 **Supplementary Figure 2 Variables affecting magnitude and shape of carbon isotope**

121 **excursion. a**, This figure is generated with the same initial conditions and parameters used in

122 Fig. 5, except we vary α_{carb} to illustrate the effect differences in the release efficiency of

carbonate C at arcs has on model carbon isotope evolution. **b**, Same as (**a**) except we vary α_{org} to illustrate the effect differences in the release efficiency of organic C at arcs has on model carbon isotope evolution. **c**, Same as (**a**) except we vary χ to illustrate the effect differences in subduction efficiency of C has on model carbon isotope evolution. **d**, Same as (**a**) except we vary τ_{OIB} to illustrate the effect differences in the delay time for the release of organic C at OIBs has on model carbon isotope evolution. **e,** same as (**a**) except we vary the magnitude of the increase in MOR CO_2 emissions. Note that at large magnitudes of CO_2 increase the magnitude of C isotope excursions becomes insensitive the magnitude of the change in CO_2 emissions, *i.e.* the curves for 100-fold and 1000-fold increase in CO_2 emissions create the same magnitude of C isotope excursion.

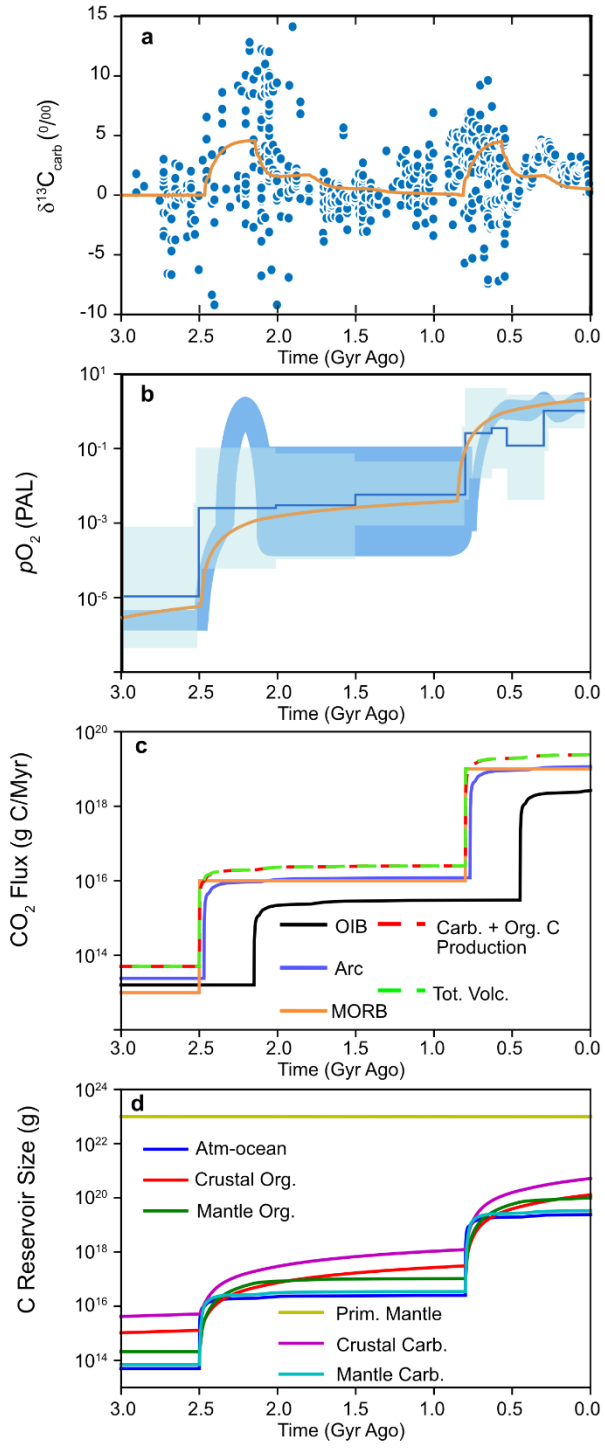

133

134 **Supplementary Figure 3 Increasing CO_2 Emissions to present day** Same as Fig. 5 of main

135 text, but with a second increase in MOR emissions from 10^{16} g/Myr to 10^{19} g/Myr which is close

136 to present estimates[41]. Note that if CO_2 emissions are set close to present-day estimates, then O_2

levels are close to present day levels. Additionally, model dependent C reservoirs (**d**) and fluxes (**c**) are similar to values for the present-day Earth. Prescribing a second increase in CO_2 emissions generates a second carbon isotope excursion and increase in oxygen, which is observed in the natural data at the end of the Proterozoic. This demonstrates that the mechanism described here may explain other important times in Earth history in addition to the GOE and LE.

Supplementary Table 1 Initial conditions and parameters used in model run to generate Fig. 5

Initial Conditions	**Value**	**Units**
$C_{atm}(0)$	0	[g]
$C_{carb}(0)$	0	[g]
$C_{org}(0)$	0	[g]
$C_{mcarb}(0)$	0	[g]
$C_{morg}(0)$	0	[g]
$C_{prm}(0)$	10^{23}	[g]
F_{MORB}, F_{Arc}, F_{OIB}	10^{13}	[g/Myr]
Parameters		
f_{org}	0.2	-
k	0.1	[Myr^{-1}]
χ	0.6	-
α_{carb}	1	-
α_{org}	0	-
κ_1	10^{13}	[g/Myr]
κ_2	10^{13}	[g/Myr]
$\delta^{13}C_{prm}$	-5	-
τ_{arc}	30	Myr
τ_{OIB}	350	Myr
dt	1	Myr

At the start of the model, all C is held in the primitive mantle reservoir with other reservoirs holding no C. Very quickly the other C reservoirs stabilize at a steady-state value in response to the initial volcanic CO_2 fluxes (Fig. 5c,d and Supp. Fig. 3c,d)

Supplementary Table 2 C isotopes of arc CO_2 emissions and f_{org} of sediments used to generate Fig. 2a

Arc	$\delta^{13}C$	σ	f_{org} of subducting sediments
Kermadec	-2.8	0.8	0.08
Kuril-Kamchatka	-6.1	1.1	0.75
Cascades	-8.6	1.2	0.57
Guatemala	-2.9	0.1	0.10
Mexico	-6.3	0.0	0.63
Nicaragua	-2.8	0.6	0.13
Costa Rica	-4.1	1.4	0.12
Colombia	-6.9	1.7	0.14
N. Chile	-4.1	2.6	0.17
Aleutians	-7.0	2.0	0.38
Lesser Antilles	-4.3	0.5	0.22
Java	-3.7	0.8	0.06
SW Japan	-5.9	1.4	0.41
NE Japan	-3.8	1.1	0.89
Aegean	-2.4	1.0	0.61

$\delta^{13}C$ is the mean of all $\delta^{13}C$ measured at individual volcanoes from a particular arc (Data from Ref. [22]). σ is one standard deviation of the mean $\delta^{13}C$ for a particular arc. f_{org} of subducting sediments is the ratio of organic carbon to carbonates for a specific arc (Data from Ref. [48]). Arcs marked as orange dots in Fig. 2a, indicating significant upper plate carbonate assimilation are NE Japan and Aegean arcs.

Supplementary Table 3 $\delta^{13}C$ data for intraplate ocean island volcanoes used in Fig. 3

Reference	Location	Sample Type	$\delta^{13}C$	CO_2 (ppm)
Hauri (2002)[35]	Koolau	melt inclusion	-29.0	234
			-18.0	177
			-12.0	**563**
Aubaud et al. (2005)[23]	Society	vesicle	-5.7	562
			-4.2	224
			-5.2	53
			-6.8	136
			-7.1	36
			-7.2	127
			-6.3	131
			-3.8	**1487**
			-4.1	995
			-7.7	4
			-7.0	6
			-6.6	8

			-6.1	120
			-6.2	43
			-6.1	75
			-6.7	130
			-6.7	49
			-6.8	11
			-9.7	1
			-8.0	11
			-8.6	57
			-5.0	18
			-4.9	25
			-4.9	21
			-6.8	24
			-5.7	27
			-5.3	69
Aubaud et al. (2006)[21]	Pitcairn	vesicle	-13.5	11
			-13.0	10
			-13.9	21
			-6.7	820
			-9.3	70
			-10.8	66
			-10.6	23
			-11.5	17
			-6.7	470
			-6.7	**870**
			-7.0	500
			-7.0	680
			-7.6	100
			-7.0	18
			-15.7	6
			-7.9	76
			-8.2	37
			-9.5	37
			-9.1	115
			-10.0	61
			-9.3	65
			-9.9	88
			-7.5	36
			-11.5	2
			-15.7	12
			-11.8	2
			-10.9	16
			-10.7	51

			-14.4	12
			-10.1	69
			-7.6	39
			-12.3	7
			-10.0	9
			-12.1	10
			-6.0	270
Exley et al. (1986)[36]	Loihi	glass chips	-6.9	147
			-13.7	55
			-15.0	59
			-12.1	51
			-17.3	**220**
			-15.6	85
			-16.6	148
			-19.3	32
Gerlach & Taylor (1990)[34]	Kilauea	volcanic gases	-8.9	n/a
			-7.3	n/a
			-7.6	n/a
			-8.5	n/a
			-7.4	n/a
			-7.5	n/a
			-6.9	n/a
			-8.9	n/a
			-7.4	n/a

Values marked in bold are least degassed samples for a particular dataset, which are marked with stars in Fig. 3

Supplementary Table 4 Sediment partial melt compositions used in Supp. Fig. 1.

Oxide	Dobson et al., 1989[60]	Tsuno & Dasgupta, 2012[61]	Duncan & Dasgupta, 2017[27]
SiO_2	77.70	59.67	68.77
TiO_2	0.07	0.62	0.56
Al_2O_3	13.00	12.45	15.71
FeO	0.38	6.09	0.99
MnO	0.04	0.17	0.50
MgO	0.05	2.46	0.19
CaO	0.52	8.01	1.47
Na_2O	4.08	2.23	4.19
K_2O	4.19	1.97	7.33

References

14. Fuentes, J. J., Crowley, J. W., Dasgupta, R. & Mitrovica, J. X. The influence of plate tectonic style on melt production and CO2 outgassing flux at mid-ocean ridges. *Earth Planet. Sci. Lett.* **511**, 154–163 (2019).

17. Sobolev, S. V & Brown, M. Surface erosion events controlled the evolution of plate tectonics on Earth. *Nature* **570**, 52–57 (2019).

21. Aubaud, C., Pineau, F., Hékinian, R. & Javoy, M. Carbon and hydrogen isotope constraints on degassing of CO_2 and H_2O in submarine lavas from the Pitcairn hotspot (South Pacific). *Geophys. Res. Lett.* **33**, L02308 (2006).

22. Mason, E., Edmonds, M. & Turchyn, A. V. Remobilization of crustal carbon may dominate volcanic arc emissions. *Science.* **357**, 290–294 (2017).

23. Aubaud, C., Pineau, F., Hékinian, R. & Javoy, M. Degassing of CO_2 and H_2O in submarine lavas from the Society hotspot. *Earth Planet. Sci. Lett.* **235**, 511–527 (2005).

24. Keller, C. B. *et al.* Neoproterozoic glacial origin of the Great Unconformity. *Proc. Natl. Acad. Sci.* **116**, 1136–1145 (2019).

27. Duncan, M. S. & Dasgupta, R. Rise of Earth's atmospheric oxygen controlled by efficient subduction of organic carbon. *Nat. Geosci.* **10**, 387–392 (2017).

32. Li, M. & McNamara, A. K. The difficulty for subducted oceanic crust to accumulate at the Earth's core-mantle boundary. *J. Geophys. Res. Solid Earth* **118**, 1807–1816 (2013).

34. Gerlach, T. M. & Taylor, B. E. Carbon isotope constraints on degassing of carbon dioxide from Kilauea Volcano. *Geochim. Cosmochim. Acta* **54**, 2051–2058 (1990).

35. Hauri, E. SIMS analysis of volatiles in silicate glasses, 2: isotopes and abundances in Hawaiian melt inclusions. *Chem. Geol.* **183**, 115–141 (2002).

36. Exley, R. A., Mattey, D. P., Clague, D. A. & Pillinger, C. T. Carbon isotope systematics of a mantle 'hotspot': a comparison of Loihi Seamount and MORB glasses. *Earth Planet. Sci. Lett.* **78**, 189-199 (1986).

41. Dasgupta, R. & Hirschmann, M. M. The deep carbon cycle and melting in Earth's interior. *Earth Planet. Sci. Lett.* **298**, 1–13 (2010).

45. Williams, J. J., Mills, B. J. W. & Lenton, T. M. A tectonically driven Ediacaran oxygenation event. *Nat. Commun.* **10**, 2690 (2019).

48. Clift, P. D. A revised budget for Cenozoic sedimentary carbon subduction. *Rev. Geophys.* **55**, 97–125 (2017).

55. Eguchi, J. & Dasgupta, R. A CO_2 solubility model for silicate melts from fluid saturation to graphite or diamond saturation. *Chem. Geol.* **487**, 23–38 (2018).

56. Caves, J. K., Jost, A. B., Lau, K. V. & Maher, K. Cenozoic carbon cycle imbalances and a variable weathering feedback. *Earth Planet. Sci. Lett.* **450**, 152–163 (2016).

57. Berner, R. A. GEOCARBSULF: A combined model for Phanerozoic atmospheric O2 and CO2. *Geochim. Cosmochim. Acta* **70**, 5653–5664 (2006).

58. Falkowski, P. *et al.* The global carbon cycle: A test of our knowledge of earth as a system. *Science* **290**, 291–296 (2000).

59. Berner, R. A., Lasaga, A. C. & Garrels, R. M. The carbonate-silicate geochemical cycle

and its effect on atmospheric carbon dioxide over the past 100 million years. *Am. J. Sci.* **283**, 641–683 (1983).

60. Dobson, P. F., Epstein, S. & Stolper, E. M. Hydrogen isotope fractionation between coexisting vapor and silicate glasses and melts at low pressure. *Geochim. Cosmochim. Acta* **53**, 2723–2730 (1989).

61. Tsuno, K. & Dasgupta, R. The effect of carbonates on near-solidus melting of pelite at 3 GPa: Relative efficiency of H2O and CO2 subduction. *Earth Planet. Sci. Lett.* **319**–**320**, 185–196 (2012).